8.A.8 Nuclear Physics B 11 (1969) 479-494. North-Holland Publ. Comp., Amsterdam

LONGITUDINAL PHASE SPACE ANALYSIS OF THREE-BODY FINAL STATES IN MESON-NUCLEON COLLISIONS

A. BIAŁAS *, A. ESKREYS **, W. KITTEL ***, S. POKORSKI ‡, J. K. TUOMINIEMI ⌗ and L. VAN HOVE

CERN - Geneva

Received 12 May 1969

Abstract: The longitudinal phase-space analysis is applied to various three-body final states of meson-nucleon collisions at 5-16 GeV/c primary momentum. The distributions of the angle ω along the hexagonal phase space plot and the dependence of average transverse momenta on ω are investigated in some detail. From the very rich structure of the ω distributions it is possible to conclude that, whenever allowed, the diffraction mechanism (single Pomeranchuk exchange) dominates the three-body reactions at high energy. The study of the transverse momentum distributions reveals the existence of strong correlations between longitudinal and transverse momenta which cannot be explained by phase-space effects. Some consequences of our analysis for the Regge-exchange models are briefly mentioned.

1. INTRODUCTION

The present paper applies the method of longitudinal phase space plots, as presented in our previous paper †, to various three-particle final states of πp and Kp collisions. We have studied the following reactions:

(a) $\pi^+ p \to \pi^+ \pi^0 p$, at 8 GeV/$c$,

(b) $\pi^+ p \to \pi^+ \pi^+ n$, at 8 GeV/$c$,

(c) $K^- p \to K^0 \pi^- p$, at 10 GeV/c,

* On leave of absence from Institute of Physics, Jagellonian University and Institute of Nuclear Physics, Krakow.

** On leave of absence from Institute of Nuclear Research, Krakow.

*** CERN fellow from the Institute für Hochenergiephysik der Österreichischen Akademie der Wissenschaften, Vienna.

‡ On leave of absence from Institute of Theoretical Physics, Warsaw University, Warsaw.

⌗ On leave of absence from Department of Nuclear Physics, University of Helsinki, Helsinki.

† Ref. [1], hereafter referred to as I.

(d) $K^+p \to K^{*0}_{890}\pi^+p$, at 5 GeV/c ,

(e) $K^+p \to K^{*++}_{890}\pi^0p$, at 5 GeV/c ,

(f) $K^+p \to K^0\pi^+p$, at 5 GeV/c ,

(g) $\pi^+p \to \pi^+\pi^-N^{*++}$, at 8 GeV/c ,

(h) $\pi^-p \to \pi^-\pi^-N^{*++}$, at 16 GeV/c ,

(i) $K^+p \to K^+\pi^-N^{*++}$, at 5 GeV/c ,

(j) $K^+p \to K^0\pi^0N^{*++}$, at 5 GeV/c ,

at the lab momenta indicated. For each of them, considerable statistics was available from recent bubble chamber experiments carried out by the Aachen-Berlin-CERN, Aachen-Berlin-CERN-London (I.C.)-Vienna, Aachen-Berlin-Bonn-CERN-Heidelberg and CERN-Brussels collaborations ‡.

We recall briefly the definition of longitudinal phase space (LPS) plots for three-particle final states; details are found in I. The c.m. longitudinal momenta of the final particles being q_1, q_2, q_3, each event is represented by a point P in the plane of fig. 1, with distances q_i to the three lines $q_i = 0$ (these lines cut each other at angles of 60°). Events with q_i positive (negative) are plotted on the side of the $q_i = 0$ lines marked + (-). Here q_i is taken positive (negative) for a particle moving in the forward (backward) hemisphere of the c.m. system, the forward direction being by definition the direction of motion of the incident beam particles. An important variable characterizing each event in the LPS plot is the polar angle ω. As indicated in fig. 1, it is counted counter-clockwise from the line $q_1 = 0$. Be-

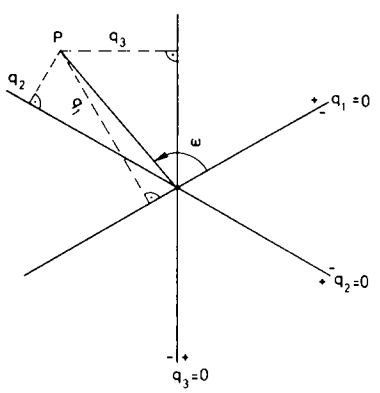

Fig. 1. The hexagonal plot.

‡ We used data from the following experiments: K^+p at 5 GeV/c, CERN-Brussels collaboration; π^+p at 8 GeV/c, Aachen-Berlin-CERN collaboration; K^-p at 10 GeV/c, Aachen-Berlin-CERN-London (I.C.)-Vienna collaboration; π^-p at 16 GeV/c, Aachen-Berlin-Bonn-CERN-Heidelberg collaboration.

cause all transverse momenta of final particles remain small at high energy, the single angle ω essentially determines the complete longitudinal configuration of an event (see figs. 3 and 4 of I).

As shown in the following sections, the LPS analysis of reactions (a)-(j) reveals two striking qualitative features. The first is the occurrence of pronounced maxima in the ω distribution of events for the reactions where Pomeranchuk exchange (i.e., diffraction dissociation) is allowed, and their absence when such exchange is forbidden by internal quantum number conservation or is suppressed by parity considerations (sect. 2). The second feature emerging from the LPS analysis is the occurrence of correlations between the transverse momenta and the value of ω. These correlations appear to be strong when the ω distribution has sharp maxima (sect. 3).

We do not attempt to fit the results of the LPS analysis by means of the dynamical models now commonly used for description of three-body final states, like the double Regge model † or diffraction dissociation models [3,4]. Our theoretical considerations are limited to a few general remarks. The main one concerns the fact, clearly shown by the data, that the double Regge model cannot be regarded as a natural theoretical starting point for the description of three-particle final states. Indeed, the ω distributions are found to have their maxima where one of the three two-particle subenergies reaches its minimum, i.e., in the region of single reggeization. A double Regge description can therefore only be correct if it possesses full duality, i.e., if it gives a precise parametrization of the corresponding two-particle subsystems even at their lowest subenergy. Needless to say, no existing Regge parametrization satisfies this property. This leads us to expect that three-particle final states of high energy hadron collisions will be an excellent testing ground for Veneziano models (sect. 4).

2. DISTRIBUTIONS ALONG THE HEXAGON

We have constructed the LPS plots of all reactions (a)-(j) listed in sect. 1 Two examples for reactions (a) and (h) are given in figs. 3 and 4 of I. All ten LPS plots have in common two characteristic features clearly seen in these figures. One is the concentration of events near the kinematical border of the plot, resulting from the smallness of all transverse momenta. The other is the scarcity of events in which the final baryon has its c.m. longitudinal momentum q positive, i.e., moves in the forward hemisphere in the c.m. system. In fact, the available statistics is such that we restrict our discussion to events for which the baryon has $q < 0$. For all reactions, we allocate the variables q_1, q_2, q_3 to the three outgoing particles in the order in which they are listed in sect. 1 and in figs. 2-5 ‡. Hence q_3 refers always to the baryon and the above restriction to $q_3 < 0$ means, as seen on fig. 1, that we limit the angle ω to the interval

$$60^{\circ} < \omega < 240^{\circ} . \qquad (1)$$

† For recent reviews of the status of the multiperipheral models, see e.g. ref. [2].
‡ In all figures longitudinal c. m. momenta are denoted by p^*_L.

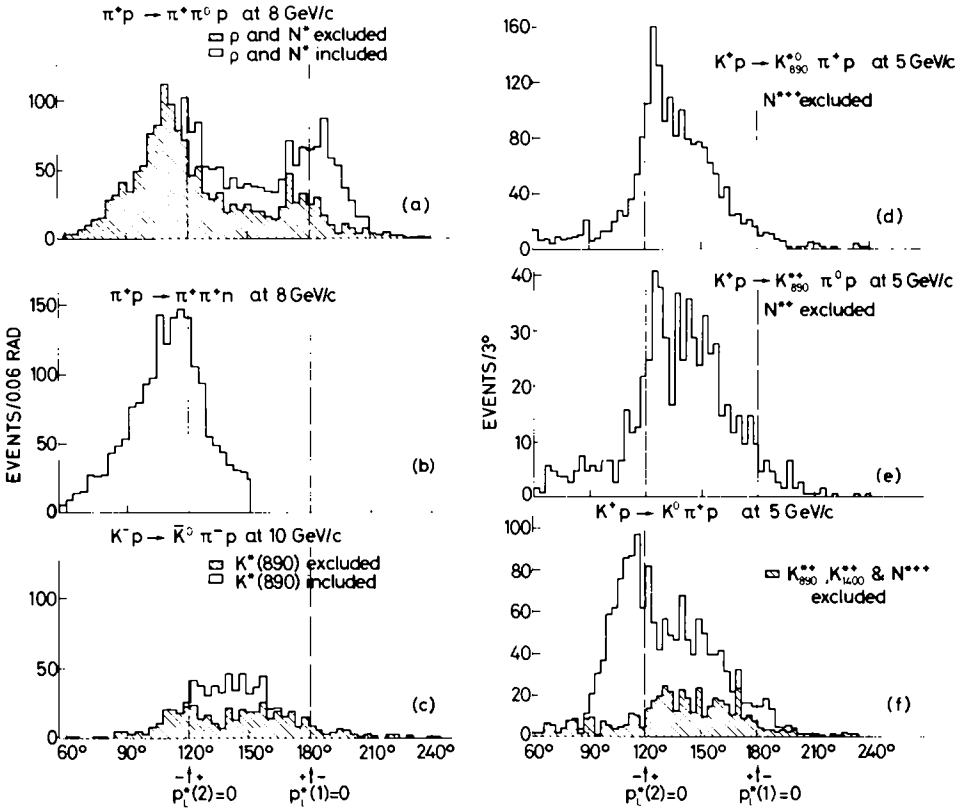

Fig. 2. Experimental distribution of the angle ω along the hexagon for the reactions (a) - (f).

An additional restriction on ω occurs for reactions (b) and (h), where the two outgoing pions are identical. All events can here be plotted in the upper half of the LPS plot. Using the restriction (1), we therefore obtain the angular interval

$$60^{\circ} < \omega < 150^{\circ} . \tag{2}$$

In this region $q_1 > q_2$, and we call $\pi_f(\pi_s)$ the pion of c.m. longitudinal momentum $q_1(q_2)$. The index refers to fast (slow) in the lab system. One has now also $|q_1| > |q_2|$, so that the c.m. velocity is larger in absolute value for π_f than for π_s.

Figs. 2 and 3 give the ω distributions of events for the ten reactions considered. In order to assess the influence of the phase space density factor in these distributions, we have replotted them in figs. 4 and 5, giving to each event the weight D_R^{-1} where D_R is the density factor given in sect. 3 of I (see figs. 7 of I for an example of the ω dependence of D_R at fixed transverse momenta). This function is easily calculated from the measured

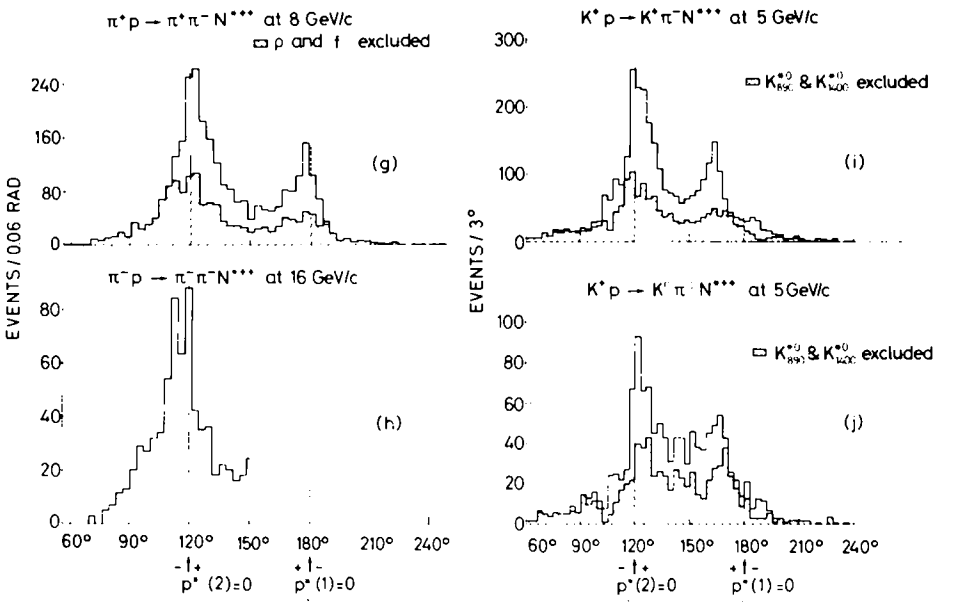

Fig. 3. Experimental distribution of the angle ω along the hexagon for the reactions (g) - (j).

momenta of each event. In terms of the (unknown) invariant matrix element M for the process, the ordinary ω distributions of figs. 2 and 3 are given by

$$\frac{\mathrm{d}N}{\mathrm{d}\omega} = \int |M|^2 D_{\mathrm{R}} \, \delta_2\Big(\sum_1^3 \boldsymbol{r}_i\Big) \prod_1^3 \mathrm{d}_2 \, \boldsymbol{r}_i \tag{3}$$

where the $\boldsymbol{r}_i$ are the transverse momenta of the outgoing particles. The weighted distributions of figs. 4 and 5, on the other hand, are given by the equation

$$\frac{\mathrm{d}N'}{\mathrm{d}\omega} = \int |M|^2 \, \delta_2\Big(\sum_1^3 \boldsymbol{r}_i\Big) \prod_1^3 \mathrm{d}_2 \, \boldsymbol{r}_i \tag{4}$$

and reflect more directly the properties of the matrix element. The main difference between the weighted and unweighted distributions is a relative lowering of the former with respect to the latter in the regions of phase space where one pion has small c.m. energy. These are the regions where D_{R} has maxima. They correspond to $\omega \approx 120^{\circ}$ for all reactions considered, and to $\omega \approx 180^{\circ}$ for reactions (a) and (g). The figures show that the weighted distributions, while still having marked structures in ω, are smoother than the unweighted ones near the special ω values mentioned, indicating that $|M|^2$ is there smoother than D_{R}.

It is clear that error estimates are less straightforward for $\mathrm{d}N'/\mathrm{d}\omega$ than for $\mathrm{d}N/\mathrm{d}\omega$ where the number of events per ω bin gives directly the main

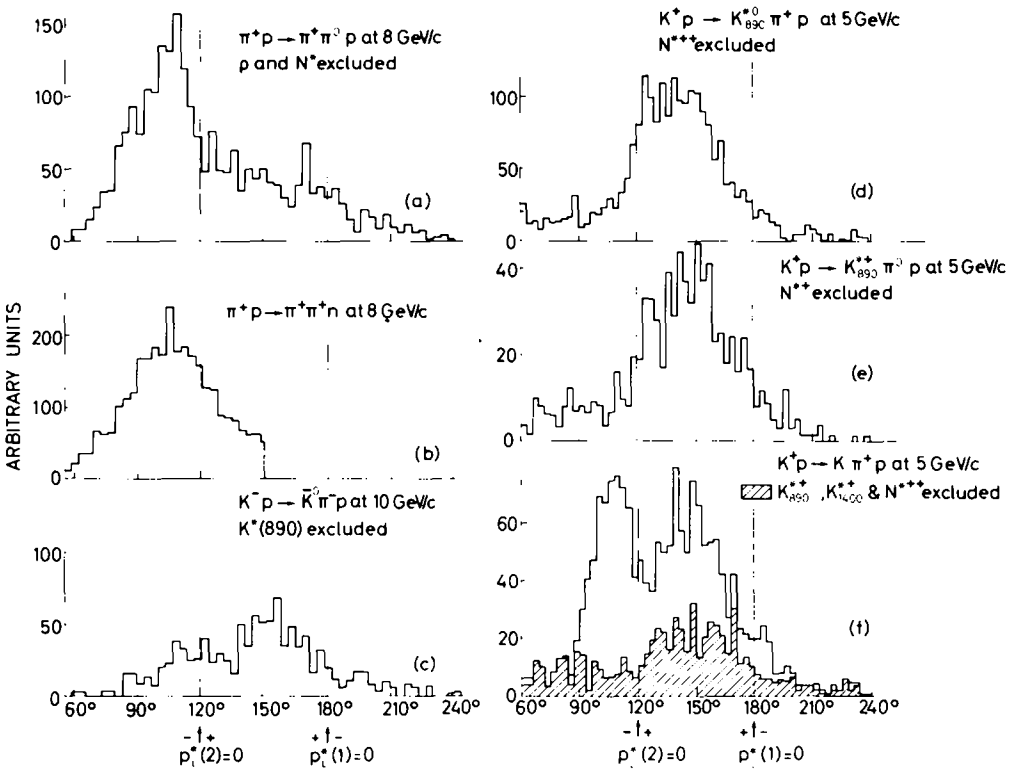

Fig. 4. Experimental distribution of the angle ω along the hexagon for the reactions (a) - (f), weighted by the longitudinal phase space.

part of the error. Away from the special angles mentioned above, however, D_R varies rather little inside a bin (a typical range would be 30%), so that the relative error on $dN'/d\omega$ will be about the same as for $dN/d\omega$. At the special angles, the relative error on $dN'/d\omega$ can be roughly estimated by interpolation from neighbouring ω values, and it is larger than the relative error on $dN/d\omega$.

The inclusion or exclusion of the most important resonances in the various ω distributions is indicated in the figures. Exclusion of a resonance means that one rejects all events with the corresponding effective mass in the following intervals:

$$\begin{aligned}
\rho \quad &: 0.66 < M(\pi\pi) < 0.86 \text{ GeV} , \\
\mathrm{f} \quad &: 1.15 < M(\pi\pi) < 1.35 \text{ GeV} , \\
\mathrm{N}^* \quad &: 1.12 < M(\mathrm{p}\pi) < 1.34 \text{ GeV} , \\
\mathrm{K}^*(890) \quad &: 0.82 < M(\mathrm{K}\pi) < 0.96 \text{ GeV} , \\
\mathrm{K}^*(1400) \quad &: 1.33 < M(\mathrm{K}\pi) < 1.51 \text{ GeV} .
\end{aligned} \tag{5}$$

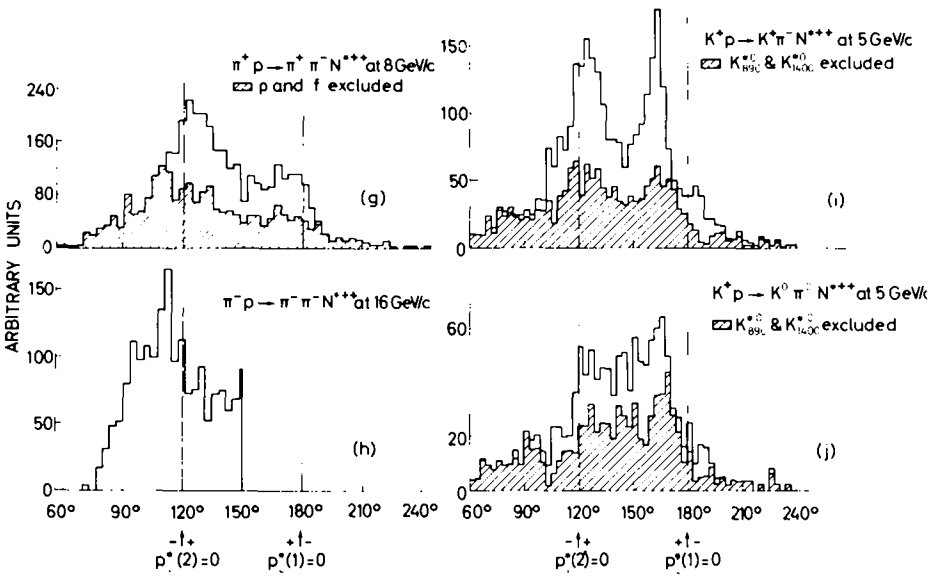

Fig. 5. Experimental distribution of the angle ω along the hexagon for the reactions (g) - (j), weighted by the longitudinal phase space.

We proceed to discuss the possible meaning of the strong structures present in the ω distributions, and do this on the weighted distributions $dN'/d\omega$ excluding resonances, in order to eliminate effects of phase space and of two-body collisions. Examination of fig. 4 reveals that the weighted ω distribution has one large and broad bump for reactions (a), (b), (d) and (e), whereas it has one broad but weaker bump for (c) and (f). The bumps are clearly localized in the interval $60^\circ < \omega \lesssim 120^\circ$ for (a) and (b), and in the interval $120^\circ < \omega < 180^\circ$ for the other four reactions.

These facts can be readily understood if we assume that the dominant mechanism in producing our final states is diffraction dissociation, i.e., Pomeranchuk or P exchange in Regge terminology. Indeed, P exchange is fully allowed in reactions (a), (b), (d) and (e) following diagram (A) for the two former ones and diagram (B) for the latter ones (see fig. 6, the numbers label the outgoing particles in the order in which they are mentioned in fig. 4). In contrast, P exchange is suppressed for reactions (c) and (f); although conservation of internal quantum numbers would allow it to proceed through diagram (B), it must be reduced by the fact that the subsystem of particles 1 and 2 has natural parity whereas the incoming kaon is pseudoscalar [5, 6]. Diagram (A) obviously implies a small subenergy s_{23} for particles 2 and 3, and indeed reactions (a) and (b) peak for $60^\circ < \omega \lesssim 120^\circ$ where this subenergy is minimum (see fig. 8 of I). Similarly, diagram (B) implies that 1 and 2 have a small subenergy s_{12}, again in agreement with the location of the bump of reactions (d) and (e) in the interval $120^\circ < \omega < 180^\circ$. As to reactions (c) and (f), they could be explained

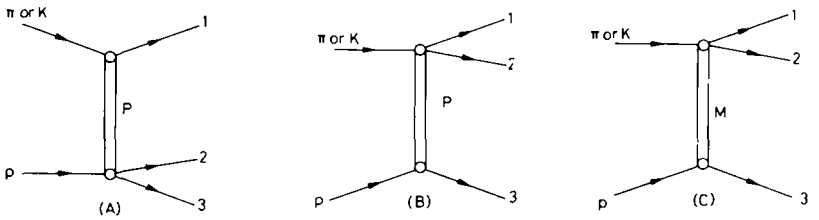

Fig. 6. Exchange diagrams giving the main contributions to the processes discussed in this paper.

by an exchange effect of the type described by diagram (C) in fig. 6, where M is a meson or Pomeranchuk cut [5] and where s_{12} takes small values.

Going over to the reactions producing N^{*++}, for which the weighted ω distributions are given in fig. 5, we see that P exchange following diagram (A) seems to dominate reactions (g) and (h) in about the same way as it does for (a) and (b). The bump is less pronounced, however, and it is shifted somewhat to the right in the case of (g). The former effect suggests that a non-diffractive mechanism plays a bigger role, the obvious candidate being again described by the diagram (C) in fig. 6, where now M is an $I = 1$ meson, presumably a pion. This diagram can be regarded as an extension of diagram (A) into the region of small s_{12}, i.e., for $120^{\circ} < \omega < 180^{\circ}$. The shift of the bump to the right for reaction (g) may be due to the importance of the contribution of diagram (C). It will also result partly from a purely kinematic effect, namely that the higher mass of N^* shifts to the right the ω meson region where s_{23} is small. Both effects should decrease at higher incident energy, and indeed the bump in the weighted ω distribution of the 16 GeV/c reaction (h) is again well on the left of $\omega = 120^{\circ}$.

For the 5 GeV/c reactions (i) and (j), while the latter does not allow P exchange and is likely to be dominated by diagram (C), the two-peak structure of the former is more puzzling and an interpretation is hard to give without information at higher energy. The left peak in fig. 5i may be well due to P exchange which is fully allowed; the low-incident energy would then be responsible for the fact that it is weak and is shifted even more to the right than for reaction (g). The second peak near $\omega = 160^{\circ}$ could presumably originate from diagram (C). If this interpretation is correct, the same reaction at higher incident energy should show an ω distribution more similar to the one of reaction (g), although it should be kept in mind that the KPK vertex is weaker than the $\pi P\pi$ one in the ratio of the total Kp and πp cross sections.

The above interpretation of the dominant structures in the distributions can and should be tested in many ways. We limit ourselves to mentioning a few lines of work, and express the hope that the information contained in existing bubble chamber data for other three-particle reactions will also be exploited for this purpose. The energy independence of cross sections dominated by P exchange can obviously be tested by comparing the appropriate ω intervals for the same reaction at various energies. Outside of the

ω intervals where P exchange dominates, cross sections should decrease with energy, giving indications on the exchange mechanisms which are there in operation; they would presumably correspond to lower lying Regge trajectories. Following Satz [7], the fact that P exchange carries isospin zero allows to compare the rates of certain reactions. Thus, reactions (a) and (b) must be in the ratio 1 to 2 if they are completely described by diagram (A) of fig. 6. While fig. 4a shows that this should not be the case (the region $\omega \gtrsim 150^{\circ}$ is too populated to be regarded as a mere tail of the bump at $\omega \lesssim 120^{\circ}$), it is interesting to note that the ratio of the partial cross section of (a) for $\omega \leq 150^{\circ}$ to the cross section of (b) is 0.51, suggesting that indeed the isospins of the subsystem (π_Sn) of (b), as well as of the subsystem (π^0p) of (a) for $\omega \leq 150^{\circ}$, are predominantly $\frac{1}{2}$. In contrast, the ratio of cross sections * for all events in (a) and (b) is 0.69.

The dependence of the partial cross-section ratio on ω is presented in fig. 7, where the quantity

$$R = \int_{60^{\circ}}^{\omega} \frac{d\sigma(a)}{d\omega'} d\omega' \Big/ \int_{60^{\circ}}^{\omega} \frac{d\sigma(b)}{d\omega'} d\omega'$$

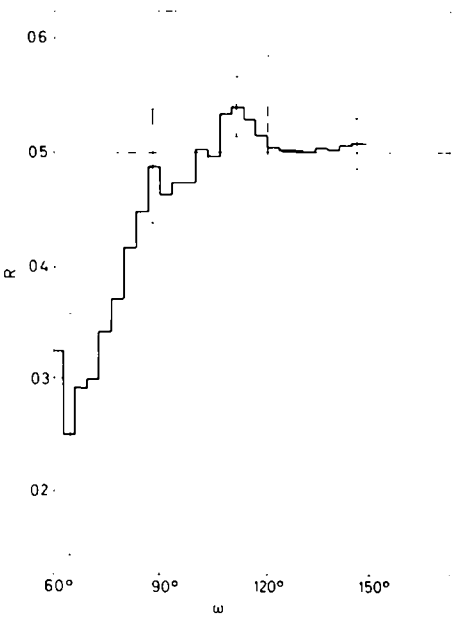

Fig. 7. The ratio $\sigma(\pi^- p \to \pi^- \pi^0 p)/\sigma(\pi^- p \to \pi^- \pi^+ n)$ as function of the angle along the hexagon, the ratio being defined as in the text.

* We used the cross-section values given by the Aachen-Berlin-CERN-collaboration [8]. For (a), we have subtracted the cross sections for production of the resonances N*, ρ, g(1650) and ρ_V(1830) as obtained in ref. [8] by fitting Breit-Wigner curves to $(p\pi^+)$ and $(\pi^0\pi^+)$ effective mass distributions. These cross sections serve as normalization to the ω distribution given in fig. 4a,b.

is plotted against ω. It is seen that in the interval $90^{\circ} \lesssim \omega < 150^{\circ}$, the ratio R is approximately constant and close to the value $\frac{1}{2}$ predicted by $I = 0$ exchange.

It is, of course, also tempting to carry out complete fits of the ω distributions by means of specific models of double Regge or diffraction dissociation type. This should not be done, however, without paying attention to the remarkable correlations between the transverse momenta and the angle ω which are described in sect. 3.

3. TRANSVERSE MOMENTUM PROPERTIES

It has often been observed that, in high energy hadron collisions, the transverse momentum distribution of each type of final particle, when taken over all events, is a rather universal function, depending little on the collision considered and on its energy. The use of LPS plots suggests to study transverse momenta p_T in a more differential way by investigating whether their properties are correlated with the longitudinal momentum configuration. For three-particle final states, this configuration is almost fully characterized by the angle ω along the hexagon.

For the reactions listed in sect. 1, we have studied, as functions of ω,

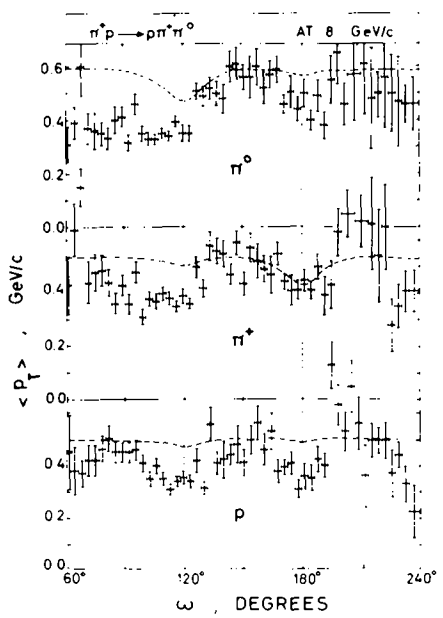

Fig. 8. Average transverse momentum as function of the angle ω for process (a). N^{*++} and ρ have been excluded. The curves represent the phase space calculations, as described in the text.

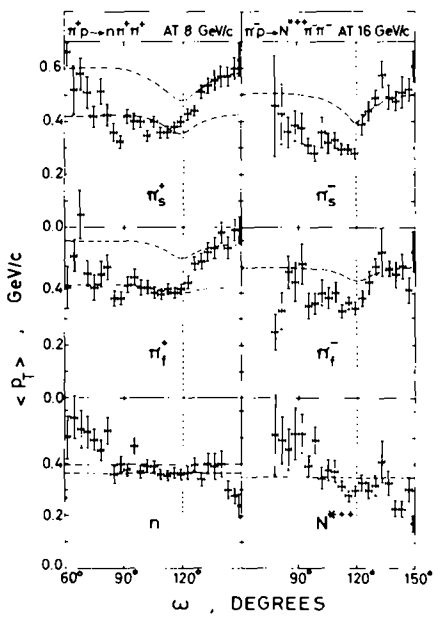

Fig. 9. Average transverse momentum as function of the angle ω for processes (b) and (h). The curves represent the phase space calculations, as described in the text.

the average values $\langle p_T \rangle$ of the transverse momenta of the final particles for events grouped by ω bins. For a few reactions, we have also determined the shape of the $\langle p_T \rangle$ distributions as well as of distributions of various angles between transverse momentum vectors, for groups of events belonging to different ω intervals. This study revealed unexpected variations of the averages and of the distributions with ω, i.e., correlations between transverse and longitudinal momentum configuration. We concentrate here on the ω dependence of the $\langle p_T \rangle$. We shall only give one example of ω dependent distributions.

Consideration of the $\langle p_T \rangle$ versus ω plots suggests an empirical rule. These plots show their strongest structure for reactions where the weighted ω distributions $dN'/d\omega$ of figs. 4 and 5 have the most pronounced maxima, and the $\langle p_T \rangle$ generally show minima at the ω values where $dN'/d\omega$ has its maximum. This is illustrated in figs. 8-10 for reactions (a), (b), (h) and (i); the resonances listed in (5) have been excluded. One indeed notices the systematic occurrence of low $\langle p_T \rangle$ in a rather narrow region at $\omega \lesssim 120^o$, where the $dN'/d\omega$ have a pronounced and rather sharp bump. Another remarkable effect exists for reactions (b) and (h) which have identical pions; it occurs at $\omega = 150^o$ where $\langle p_T \rangle$ has a maximum for pions and a minimum for the baryon (fig. 9).

The shape of the structures seen near $\omega \approx 180^o$ for reactions (a) and (i) is perhaps more difficult to assess because of the large errors on the right of this ω value (figs. 8 and 10). For the other six reactions studied in this paper the ω dependence of the $\langle p_T \rangle$ is found to be appreciably weaker. In the case of (d) which has rather high statistics, the main feature is that the $\langle p_T \rangle$ have a flat and weak minimum for $120^o \lesssim \omega \lesssim 160^o$, which is the region of the broad bump in $dN'/d\omega$.

To illustrate the effect of resonances on the $\langle p_T \rangle$ versus ω plots, we give in fig. 11 what is obtained for reaction (i) when the two K* mesons are left in the data. This strongly enhances the minima at $\omega \approx 120^o$ and gives clear minima at $\omega \approx 165^o$. As shown by fig. 3i, these ω values correspond to the two peaks observed in the resonance contribution to $dN/d\omega$ (see fig. 5i for the resonance contribution to $dN'/d\omega$). These peaks are readily understood by noting that the resonances are strongly aligned in the longitudinal direction, and it is obvious that the $\langle p_T \rangle$ of their decay products are smallest when the resonances are so aligned. Such effects can readily be produced by two-body resonances for which the momentum k of the decay products in the resonance rest frame is larger than the average $\langle p_T \rangle$ in inelastic collisions. The values of k are ≈ 0.3 and ≈ 0.6 GeV/c for K*(890) and K*(1400), respectively, so that most of the effect must be due to the latter resonance.

While heavy resonances can thus contribute minima to the $\langle p_T \rangle$ versus ω plots, it seems unlikely that they could explain all the structures observed, as shown by a comparison of figs. 10 and 11. Also reactions (b) and (h) given in fig. 8 are interesting in this respect. For them, only heavy baryon resonances could have the effect discussed above, but we note that the minima in $\langle p_T \rangle$ on the left of $\omega = 120^o$ fall in the region of $s_{23} \approx 2(\text{GeV})^2$ and $s_{13} \approx 10(\text{GeV})^2$, as can be seen by means of fig. 8 of I. Further clarity on

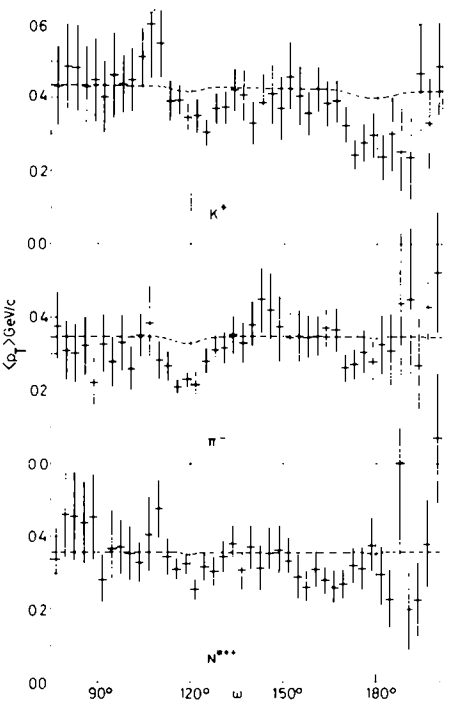

Fig. 10. Average transverse momentum as function of the angle ω for process (i). $K^*(890)$ and $K^*(1400)$ have been excluded. The curves represent the phase space calculations, as described in the text.

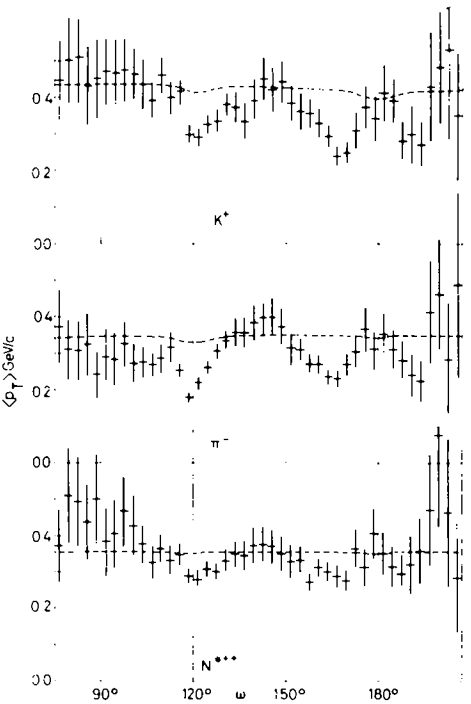

Fig. 11. Average transverse momentum as function of the angle ω for process (i) with all events included. The curves represent the phase space calculations, as described in the text.

this question will be provided by going to higher incident energies. In reaction (i) for instance, this will separate in the ω distributions (figs. 3 and 5) the peak near $\omega \approx 120^{\circ}$ produced by K^* production, which will move to the right from the peak created by P exchange, which we predict to move to the left.

We now discuss whether the structure observed in the $\langle p_T \rangle$ versus ω plots could be due to phase space effects. It should indeed be recalled that a correlation between $\langle p_T \rangle$ and the c.m. longitudinal momentum q of particles was already observed in multi-particle production processes [9, 10]. It consists in a minimum of $\langle p_T \rangle$ plotted as function of q, its position being at $q = 0$. The occurrence of this minimum for pions can be explained as an effect of the relativistic phase space density which contains the pion energy in the denominator [9, 11]. The same phase space effect operates in our plots of $\langle p_T \rangle$ versus ω. We expect it to produce a minimum in the $\langle p_T \rangle$ of a light particle for the particular ω value where the q of this particle vanishes. Transverse momentum conservation then induces weaker $\langle p_T \rangle$ minima for the other particles at the same ω. These effects are illustrated by

the curves drawn in figs. 8-11. They represent the $\langle p_T \rangle$ calculated with a matrix element of the form

$$|M|^2 = c \prod_{i=1}^{3} \exp[-a_i p_{i_T}^2] ,$$

c, a_i being constants. With such a matrix element, only phase space effects can produce correlations between transverse and longitudinal momenta. The a_i were adjusted to fit $\langle p_T \rangle$ around $\omega = 150^o$. For reaction (c)(fig. 9), a second set of curves corresponds to a fit around $\omega = 90^o$. It is clear that phase space effects do not account for the observed structures in the ω variation of $\langle p_T \rangle$, which must be attributed to the matrix elements itself. For some of our reactions, we have checked this conclusion in another way by

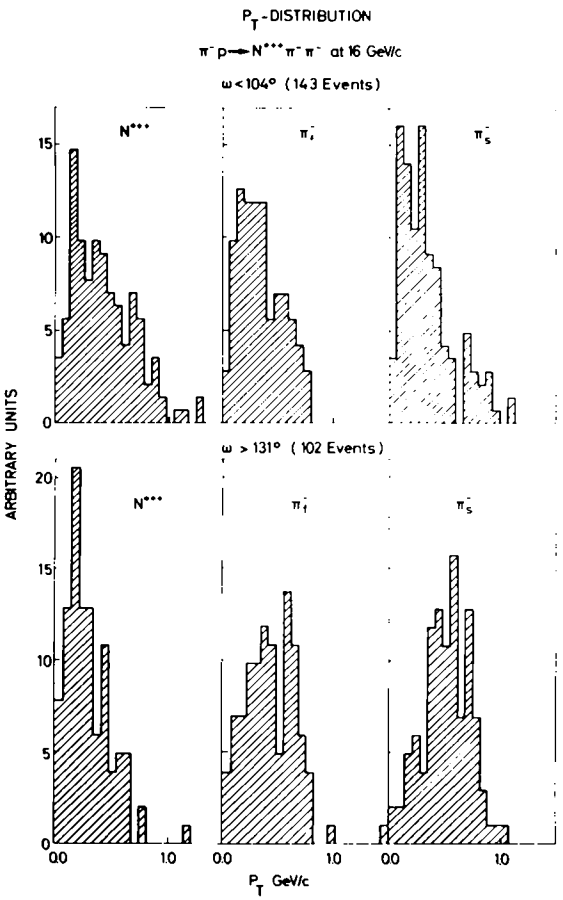

Fig. 12. Transverse momentum distributions of process (h) for two different ω intervals.

plotting from the data, as functions of ω, the weighted averages $\langle p_T \rangle'$ obtained when each event is given the weight D_R^{-1} as explained in sect. 2. In terms of the matrix element, these are

$$\langle p_{i_T} \rangle' = \left\{ \int |\boldsymbol{r}_i| |M|^2 \, \delta_2 \left(\sum_1^3 \boldsymbol{r}_j \right) \prod_1^3 \mathrm{d}_2 \boldsymbol{r}_j \right\} \Big/ \left\{ \int |M|^2 \, \delta_2 \left(\sum_1^3 \boldsymbol{r}_j \right) \prod_1^3 \mathrm{d}_2 \boldsymbol{r}_j \right\},$$

with the same notation as in eqs. (3) and (4). The structures obtained in $\langle p_T \rangle'$ are found to differ only in details from those of $\langle p_T \rangle$.

As mentioned earlier, we give only one example of ω dependence for transverse momentum distributions. It is shown in fig. 12 which contains the transverse momentum distributions of all outgoing particles for reaction (h) considered in the two following intervals of ω

$$60^\circ < \omega < 104^\circ , \qquad 131^\circ < \omega < 150^\circ .$$

One will notice the difference of range of the $\langle p_T \rangle$ distributions of the baryon and the different shapes of the $\langle p_T \rangle$ distributions of pions.

4. THEORETICAL REMARKS AND CONCLUSIONS

As mentioned earlier, this paper does not intend to present a quantitative theoretical description of the effects uncovered by the LPS analysis. We limit ourselves to some remarks of more general nature.

Considering reactions (a), (b), (d) and (e), we notice that the strong bumps in the ω distributions of fig. 4 have their maximum in the ω region where the subenergy s_{ij} of the 'diffraction dissociated' subsystem is near its minimum. This subenergy is s_{23} for reactions (a) and (b) which, we suggest, are dominated by diagram (A) of fig. 6; it is s_{12} for (d) and (e) corresponding to diagram (B) of fig. 6 (the ω dependence of s_{23} in (a) or (b) is illustrated by fig. 8 of I; the dependence of s_{12} for (d), (e) is about the same, except for the reflection $\omega \to 240^\circ - \omega$ which exchanges outgoing particles 1 and 3). We mention two related implications of this observation:

(i) It shows that the main problem connected with the use of diagrams (A) and (B) for three-body collisions is to find an adequate formula for describing a process

$$P + C_1 \to C_2 + C_3 ,$$

$$P = \text{Pomeranchuk trajectory} , \qquad C_i = \text{real particles} , \qquad (6)$$

at low and intermediate values of its own c.m. energy $\bar{s}^{\frac{1}{2}}$ ($\bar{s}$ is equal to the subenergy s_{ij} mentioned above). It is easily seen that, depending on the actual ω value within the bump of the ω distribution of the over-all reaction, the process (6) takes place either forward or backward in its own c.m. system. The double Regge model describes (6) by exchange of various Regge poles R', R" (fig. 13). It is clear that the experimental data will test such a description mainly at small $\bar{s}$ where its a priori justification is doubtful (see (ii) below). It is also clear that interference effects between the for-

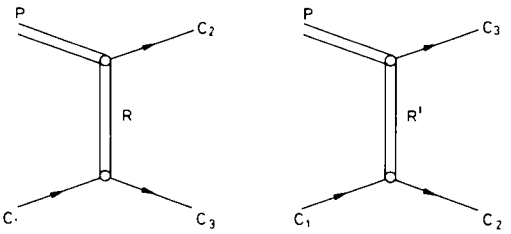

Fig. 13. Diagrams describing the interaction $P+C_1 \to C_2+C_3$ in the Regge-pole model.

ward and backward diagrams of fig. 13 will in general be essential. In addition, the duality problem has to be faced in acute form: to what degree are direct channel resonance effects (fig. 14) contained in the diagrams of fig. 13? For these various reasons, we believe that the phenomenological study of processes like eq. (6), based on a LPS analysis of three-particle collisions, could be an interesting field of application for the Veneziano model [12]. The fact that the model does not allow Pomeranchuk exchange is here inessential, because P exchange in eq. (6) is forbidden or very weak. Indeed, P exchange in eq. (6) implies double P exchange in the overall reaction, which is now known to be suppressed [13].

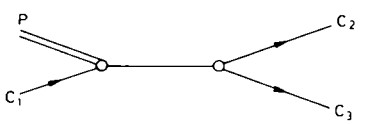

Fig. 14. Direct channel diagram contributing to the interaction $P+C_1 \to C_2+C_3$.

(ii) In many applications of the double Regge model to the analysis of three-body final states, cuts are performed on two subenergies s_{ij}, s_{jk} in order to exclude the events in which one or both of the subenergies have low values. Applied to the collisions which we have studied, this procedure amounts to keeping only the events with ω near 120^0 and those with ω near 180^0 (regions of double reggeization). The danger of testing a model on such a restricted class of events is well illustrated by considering the region $\omega \approx 120^0$ for our eight reactions allowing P exchange. In all eight cases, the region $\omega \approx 120^0$ is well inside or on the edge of the broad bump occurring in the distribution over a much wider ω region. Clearly, the theoretical description of the broad bump and of its wings cannot be separated. In other words, double Regge fits to the limited region of double reggeization can only be regarded as satisfactory if they properly describe the broader region of the bump, i.e., the region of single reggeization discussed in (i).

Regarding the correlations between the transverse momenta and the angle ω, while the $\langle p_T \rangle$ versus ω plots given in sect. 3 clearly establish their existence and location, we are not convinced that their study can be limited

to considerations of these curves. We have observed that the correlations are also very apparent when considering angular properties of the transverse momentum vectors, e.g., the shape of the triangle formed by these three vectors. Further work will be necessary before one can decide on the best choice of variables to be used for the description and theoretical fitting of the correlations in question.

For the moment, our main conclusion is of a more general nature. We believe to have established that the longitudinal phase space analysis is an effective tool for extracting the important empirical properties of three-particle final states in high energy hadron collisions, and that the most striking properties (as revealed in the ω distributions) are explainable by strong dominance of diffraction dissociation, i.e., Pomeranchuk exchange, whenever this process is allowed. We feel that the LPS analysis opens new possibilities for testing and improving quantitative dynamical models of particle production, and it will be interesting to see whether it also finds applications to final states of higher multiplicity.

We would like to thank all members of the collaborations mentioned in sect. 1 for the generous permission to make use of their unpublished data. We also thank Drs. Y. Goldschmidt-Clermont, J. D. Hansen and D. R. O. Morrison for helpful discussions.

REFERENCES

[1] L. Van Hove, Nucl. Phys. B9 (1969) 331.
[2] Chan Hong-Mo, Proc. 14th Int. Conf. on high-energy physics, Vienna (1968) p. 391;
O. Czyzewski, ibid., p. 367.
[3] M. L. Good and W. D. Walker, Phys. Rev. 120 (1960) 1857.
[4] M. Ross and Y. Y. Yam, Phys. Rev. Letters 19 (1967) 546.
[5] V. N. Gribov, Yad. Fiz. 5 (1967) 197.
[6] D. R. O. Morrison, Phys. Rev. 165 (1968) 1699.
[7] H. Satz, Phys. Letters 29B (1969) 38.
[8] M. Aderholz, M. Deutschmann, E. Keppel, G. Kraus, H. Weber, C. Grote, H. H. Kaufmann, S. Novak, M. Walter, H. Böttcher, T. Byer, V. T. Cocconi, P. F. Dalpiaz, J. D. Hansen, G. Kellner, W. Kittel, M. Markytan, A. Mihul, D. R. O. Morrison and H. Tøfte, Nucl. Phys. B8 (1968) 45.
[9] M. Bardadin-Otwinowska, L. Michejda, S. Otwinowski and R. Sosnowski, Phys. Letters 21 (1966) 351;
B. P. Bannik, B. Chadraa, A. A. Kuznetsov and N. N. Melnikova, On the correlation between longitudinal and transverse momenta of secondaries in π^-p interactions at 4 GeV/c, paper presented at the Vienna Conference (1968).
[10] V. A. Belyakov, E. N. Kladnitskaya, E. S. Kuznetsova, E. Balea, O. Balea, A. Mihul and M. Sabeu, Yad. Fiz. 5 (1967) 1232; 834.
[11] Chan Hong-Mo, J. Loskiewicz and W. W. M. Allison, Nuovo Cimento 57A (1968) 93.
[12] G. Veneziano, Nuovo Cimento 57A (1968) 190.
[13] R. Lipes, G. Zweig and W. Robertson, Phys. Rev. Letters 22 (1969) 433.